Journal of Materials Chemistry C

Accepted Manuscript

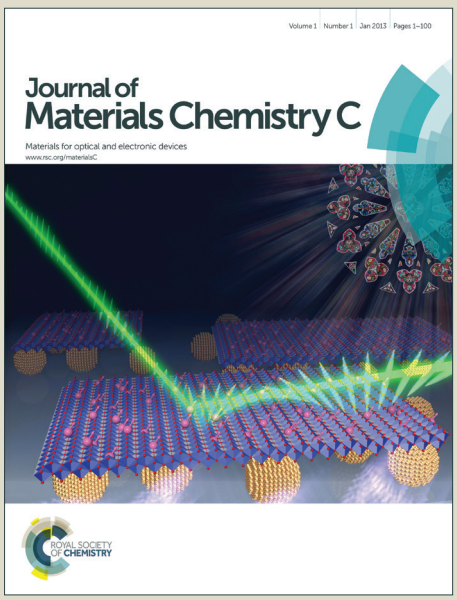

ROYAL SOCIETY OF CHEMISTRY

www.rsc.org/materialsC

Journal of Materials Chemistry C RSCPublishing

PAPER

Graphene-based gas sensor: metal decoration effect and application to a flexible device†

Cite this: DOI: 10.1039/xoxxoooooox

Received ooth January 2012,
Accepted ooth January 2012

DOI: 10.1039/xoxxoooooox

www.rsc.org/

Byungjin Cho[a]*, Jongwon Yoon[b], Myung Gwan Hahm[a], Dong Ho Kim[a], Ah Ra Kim[a], Yung Ho Kahng[c], Sang Won Park[a], Young-Joo Lee[a], Sung-Gyu Park[a], Jung-Dae Kwon[a], Chang Su Kim[a], Myungkwan Song[a], Yongsoo Jeong[a], Kee-Seok Nam[a], Heung Cho Ko[b]

Roles of metal nanoparticles (NPs) on graphene-based devices were investigated in terms of gas sensing characteristics of NO_2 and NH_3, and flexible gas sensor was also realized for futuristic sensing applications. The synergistic combination of metal NPs and graphene modulates the electronic properties of graphene, leading to the enhancement of selectivity and sensitivity in gas sensing characteristics. Introduction of palladium (Pd) NPs on the graphene accumulates hole carriers of graphene, resulting in the gas sensor sensitized by NH_3 gas molecular adsorption. Contrariwise, aluminum (Al) NPs deplete hole carriers, which improves dramatically NO_2 sensitivity. Furthermore, sensitivity of flexible graphene-based gas sensor was also enhanced *via* the same approach even after 10^4 bending cycles and then 3 months.

Introduction

In last few decades low-dimensional nanomaterials have been developing dramatically in cutting-edge technology. Obviously, graphene is the middle of momentous advances. Owing to its extraordinary physical properties,[1–5] graphene has stimulated considerable interests in diverse potential applications: transistors,[6] high-frequency electronics,[7,8] energy conversion,[9] photo detector,[10] field emission display,[11] gas sensor,[12,13] and transparent conductors.[14] In particular, its structural advantages like high surface-to-volume ratio can be translated into highly sensitive gas sensor applications *via* the adsorption/desorption of gas molecules.[12,15–25] Novoselov et al. first reported the gas sensing capability of mechanically exfoliated graphene sheets for NO_2 and NH_3.[12] Meanwhile, lots of research works have been mainly focused on the improvement of gas sensitivity using graphene. Recently, sensitivity of the graphene-based chemical gas sensors have been improved by using functionalized graphene with metal,[16,20] metal oxide,[15] or polymer.[22] Structural modification of graphene utilizing three-dimensional graphene foam[19] or nanomesh network[17] could be also another approach to implement highly sensitive gas sensors. Nevertheless, it is a critical step not only to realize selective gas sensors utilizing tunable electronic properties but also to elucidate its underlying mechanism. Furthermore, based on the studies proposed above, flexible gas sensing applications with high performance should be also realized.

In this work, we elucidated the roles of metal nanoparticles (NPs) on graphene in term of sensing behavior of NO_2 and NH_3, and demonstrated flexible gas sensor application as well. Palladium (Pd) NPs slightly improved NH_3 selectivity to NO_2. On the contrary, selectivity of NO_2 to NH_3 was drastically enhanced by the decoration of aluminum (Al) NPs. Experimental approaches substantiate that the synergetic combination of metal NPs and graphene accumulates or depletes hole carriers, thereby assisting the device either sensitized or ineffective towards molecular adsorption. In addition, robust and flexible graphene-based gas sensor with high sensitivity was demonstrated. The flexible sensing device showed excellent gas sensing characteristics even after 10^4 bending cycles and long-term stability after 3 months was also reasonably maintained.

Experimental Section

Growth of multilayer graphene

Ni/Ti film (300/30 nm) was deposited on a 4-inch Si wafer with 300 nm thick SiO_2 film by using e-beam evaporator. The wafer was positioned in the center of quartz tube and then annealed at 300 °C under the pressure of 800 Torr for 30 min with Ar (2,000 sccm)/H_2 (80 sccm) to remove the oxidized layer on the Ni film. When the temperature reached 900 °C, the graphene film was grown on the Ni film under the flow of Ar (2,000 sccm)/H_2 (80 sccm)/CH_4 (20 sccm) for 5 min, and then the quartz tube was cooled down.

Fabrication of gas sensor devices

Fig. S1 in Supplementary Information (SI) shows sequential fabrication process of graphene-based gas sensor devices.

Firstly, SiO_2/Si or polyimide (PI) was prepared as substrates for the devices, followed by typical cleaning process. For transfer of graphene films grown on Ni film to the prepared substrate, the graphene samples with area of 5 × 5 mm^2 were prepared. Poly(methyl methacrylate) (950K PMMA A2, MicroChem) as a supporting layer was spin-coated with 3,000 rpm for 35 sec. The Ni film was etched by an aqueous $FeCl_3$ solution. The multilayer graphene film with the supporting layer was transferred to hard SiO_2/Si or flexible PI substrate, and dried at 60 °C on a hotplate. After that, the supporting layer was removed by acetone. Using a shadow mask with interdigitated electrode (IDE) array structure consisting of two opposing comb-shaped electrodes of 400 μm width and 100 μm gap, Au/Ti film (100/7 nm) was deposited on the transferred graphene film by a sputter coater. Basically, the formation method of metal NPs on graphene on the flexible substrate was exactly the same as that on SiO_2/Si hard substrate. Using a thermal evaporator, we could simply form metal NPs which are randomly distributed on a graphene film. Specifically, Pd or Al metal with very thin thickness of 1 nm, monitored by a quartz crystal thickness monitor, was deposited on the graphene at deposition rate of ~ 0.3 Å/s under pressure of ~5 × 10^{-6} torr. Pd or Al NPs were naturally formed on graphene film without any post-treatment. Actual substrate temperature during Pd or Al decoration process was below 40 °C. The effect of the low temperature on graphene film would be negligible. Gas sensing device using bare graphene was also fabricated as a control group.

Gas sensing measurement

Gas sensing test was conducted by exposing the gas sensor devices to analyte gas (NO_2 or NH_3 gas) diluted with dry air in a closed chamber for 5 min. The concentrations of the analyte gases were adjusted by flow rate ratio of both gases (air and analyte gas). For recovery of the sensor, dry air was supplied into the chamber for 30 min. Using Keithley 2401 source meter, a sensing signal of the resulting gas sensing devices was checked by monitoring the resistance value measured at the voltage of 10 mV. Operation temperature of 150 °C was selected for optimizing gas sensitivity and recovery.

4-probe Hall measurement

Room temperature Hall effect measurements of graphene-based films were performed using the Van der Pauw method in a commercial Lakeshore 8404 system under a reversible magnetic of 610 G. All the Hall voltages were obtained with an error of 10 % or less. From the measurement, several electrical parameters (type of carrier, mobility, carrier concentration, resistivity, sheet resistance, and hall coefficient which are denoted as type, μ, n, ρ, R_s, and R_H, respectively) could be extracted as shown in Table S1 in the SI.

Current-voltage (I-V) electrical test

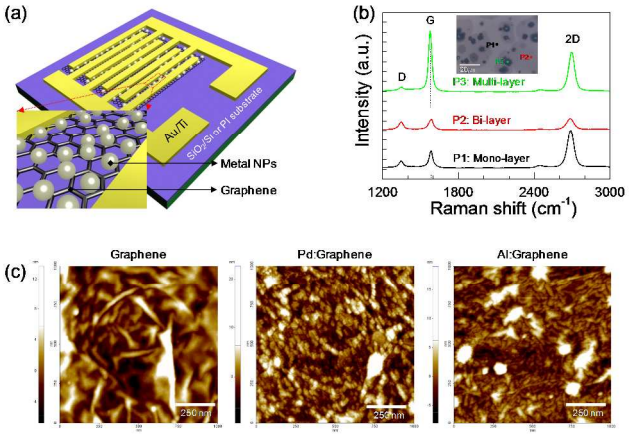

Fig. 1 (a) 3D schematic image of graphene-based devices with interdigitated electrodes and graphene channel decorated with metal NPs. (b) Raman spectra of mono-, bi-, and multi-layer of graphene film; inset: optical microscope image of graphene film displaying P1 (black closed circle), P2 (red closed circle), and P3 (green closed circle) points for Raman measurement. (c) AFM morphology images of Graphene, Pd:Graphene, and Al:Graphene.

I-V curves of graphene-based devices were obtained using a Keithley 2636A source meter under dark condition. The same devices used for gas sensing test were tested with sweep range of ±1 V and step voltage of 100 mV. Maximum compliance current of 100 mA was allowed for the test.

Results and discussion

Fig. 1a shows a schematic image of a graphene-based device with Au/Ti IDE array on substrate (hard Si/SiO_2 substrate or flexible PI substrate) and inset image of a graphene channel decorated with Pd or Al metal NPs. Fig. 1b represents Raman spectra measured from each different point (P1, P2, and P3 on the inset of Fig. 1b) of graphene film which could be distinguished by contrast difference. The graphene, synthesized by chemical vapor deposition method, has three typical bands which are D, G, and 2D band, corresponding to ~1346 cm^{-1}, ~1583 cm^{-1}, ~2688 cm^{-1}, respectively. The D band indicates the breathing mode of the rings of sp^2-hybridized carbon.[26] Its intensity reflects graphene quality because it is activated by the presence of defects and disorders of plane.[27] The G band is related to the in-plane vibration of sp^2 C atoms in single-layer graphene[28] and the 2D band is very sensitive to the stacking order along the c- axis of graphene.[29] Therefore, the thickness in graphene-based materials can be estimated from the intensity ratio of 2D to G band I_{2D}/I_G as follows: I_{2D}/I_G ~2 for mono-layer, I_{2D}/I_G ~1 for bi-layer and I_{2D}/I_G < 1 for multi-layer.[30] The raman sepctra indicate that synthesized graphene has mono-, bi-, and multi-layer. As shown in Fig. 1b, the relatively low intensity of D band in graphene indicates low density of defects. Fig. S2 in the SI displays an Atomic Force Microscopy (AFM) image and line profile of the graphene film transferred to SiO_2/Si substrate, which also indicates that its thickness is less than approximately 15 nm. AFM images show surface morphologies of bare graphene and metal decorated graphene (denoted as Graphene, Pd:Graphene, and Al:Graphene) as

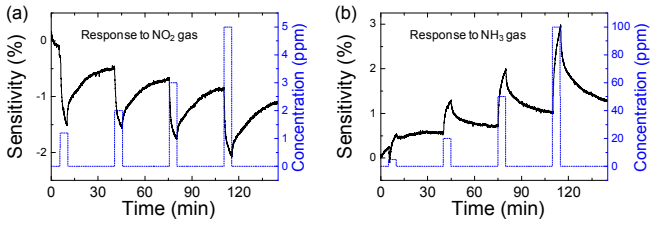

Fig. 2 Transient gas sensing characteristics of Graphene device. (a) Responses to NO_2 gas from 1.2 to 5 ppm. (b) Responses to NH_3 gas from 5 to 100 ppm. All the gas sensing test was performed at the operating temperature of 150 °C.

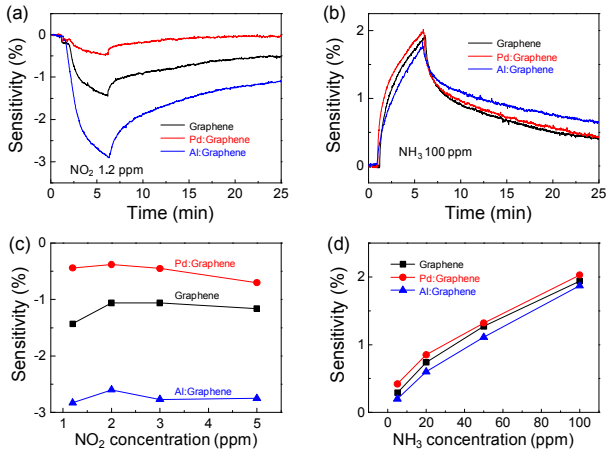

Fig. 3 Gas sensitivity of Graphene, Pd:Graphene, and Al:Graphene devices. (b) Transient response upon 1.2 ppm of NO_2 gas (b) Transient response upon 100 ppm of NH_3 gas. (c) Sensitivity under the NO_2 concentration from 1.2 to 5 ppm. (d) Sensitivity under the NH_3 concentration from 5 to 100 ppm. All the gas sensing test was performed at the operating temperature of 150 °C.

shown in Fig. 1c. The surface of the Graphene has some wrinkles, but its surface morphology is overall smooth. Pd:Graphene has uniformly distributed discrete Pd NPs with ~40 nm in size. On the other hand, in the case of Al:Graphene, Al NPs form complex morphology consisting of irregular-shaped islands of ~100 nm in size. The distinct difference (in terms of size and shape) of the morphologies may be explained by different interaction between graphene and metals.[31,32] Weak interaction between Pd metal and graphene forms fine NPs; however, stronger interaction of Al metal with graphene forms larger-grain sized NPs, indicating high nucleation rate and low surface diffusion rate of absorbed Al metal atoms on graphene. Note that Al can be easily oxidized, indicating formation of natively oxidized AlO_x shell-Al NPs.[32]

In order to demonstrate the potential utility of gas sensing property on Graphene device, we measured its resistance change exposed to analyte gases (NO_2 or NH_3). Sensitivity was defined as $\Delta R/R_a = (R_g - R_a)/R_a$, where R_a and R_g represents the resistance of the sensor to be exposed to air and analyte gas, respectively. It has been well known that the desorption process of gas molecules adsorbed on sensing graphene film can be accelerated by annealing.[33] As shown in Fig. S3a in the SI, the sensing characteristics of NO_2 gas was strongly depend on operating temperature. With increasing temperature from 27 to 200 °C, the sensitivity under NO_2 1.2 ppm flow was gradually increased from 0.3 to 0.9 (specifically, the sensitivity was rapidly increased in the range of 50 ~ 100 °C and over the temperature range, its value was saturated) while recovery percentage calculated at 35 min after turning off NO_2 gas reached approximately ~100% at 150 °C, which indicates full recovery to initial baseline resistance (see Fig. S3b in the SI). Thus, 150 °C was selected as operating temperature for following gas sensing tests. Fig. 2a displays the sensitivity of Graphene device under increasing NO_2 gas concentration of 1.2, 2, 3, and 5 ppm (right Y-axis in Fig. 2a). Upon exposure to NO_2 gas, it showed negative sensitivity (i.e., the resistance decreased). After the NO_2 gas was turned off, the sensitivity could recover to the base line under air flow even though slight baseline down-shifted. On the other hand, the sensitivity upon exposure to NH_3 gas showed positive sign (i.e., the resistance increased) as shown in Fig. 2b. Meanwhile, limit of detection (LOD) under NO_2 gas was much lower than that of NH_3 gas because the response below 5 ppm concentration of NH_3 gas was negligible (data not shown here). With increasing NH_3 concentration ranging from 5 to 100 ppm (right Y-axis in Fig. 2b), the sensitivity also was gradually increased. NO_2 and NH_3 analyte gas has been considered as electron acceptor and electron donor molecule, respectivelyter.[12] And, graphene film is p-type material with holes as major carriers under ambient condition originating from adsorbed water or oxygen molecules.[34] Thus, upon exposure to NO_2, hole carriers in graphene are accumulated (i.e., resistance decreased) through the electron charge transfer process from graphene to NO_2 gas molecules. Contrarily, in the case of NH_3 gas, electron charge transfer from NH_3 to graphene depletes hole carriers in graphene (i.e., resistance increased). In the meantimes, the lower LOD for NO_2 gas is derived from the higher adsorption energy of NO_2 molecules compared to that of NH_3 molecules.[21,35] It has been already theoretically verified that graphene gas sensors have commonly been shown to be more sensitive to NO_2 than NH_3 because of high adsorption energy (182 meV) and large charge transfer energy (0.182e from graphene to molecule) of NO_2 compared to NH_3 (adsorption energy of 29 meV and charge transfer energy of 0.008e from molecule to graphene).[36]

In order to investigate the effect of metal decoration on graphene in gas sensing property, we have fabricated three kinds of sensing devices with bare graphene and graphene decorated with Pd or Al NPs (denoted as Graphene, Pd:Graphene, and Al:Graphene device, respectively) and measured gas response characteristic of each device. Upon 1.2 ppm concentration of NO_2 gas, sensitivity of the Al:Graphene device was enhanced by around 200 % (from 1.44 to 2.89) compared to the Graphene device. In the case of the Pd:Graphene device, its sensitivity was decreased around 32 % (from 1.44 to 0.46) (Fig. 3a). On the other hand, in the case of 100 ppm NH_3 gas sensitivity, compared to Graphene device, Pd:Graphene device was slightly increased (from 1.94 to 2.04); however, Al:Graphene device was decreased (from 1.94 to 1.87) (Fig. 3b). The results show totally different tendency with NO_2

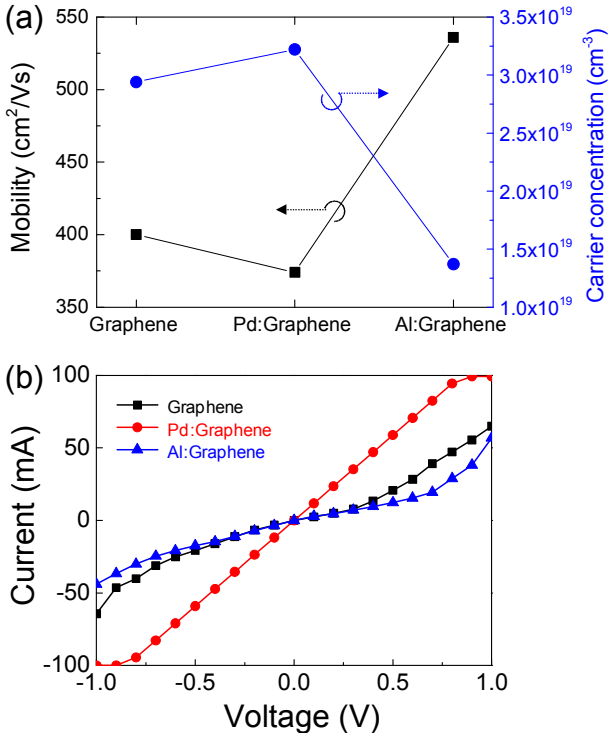

Fig. 4 (a) Mobility and carrier concentration. (b) I-V electrical characteristics of Graphene, Pd:Graphene, and Al:Graphene devices.

gas response. Additionally, we confirmed the gas response characteristics under different concentrations. With increasing concentration from 1 to 5 ppm NO_2 gas, it was clearly observed that Al:Graphene shows exceptional sensing characteristic, indicating the decoration of Al NPs on graphene film is effective to detect NO_2 gas as shown in Fig. 3c. With increasing from 5 to 100 ppm NH_3 gas, Pd:Graphene device was effective for detecting NH_3 as shown in Fig. 3d. In particular, NH_3 sensitivities of all the devices were linearly increased, indicating the correlation between gas response and gas concentration was in good agreement with the Langmuir adsorption isotherm model.[37] Compared to NO_2, weak response of NH_3 might result from weak chemical reaction between graphene and NH_3 gas, and the absence of the enhanced roles from metal decoration.[36] Irrespective of a kind of metal decorated, the relatively stronger adsorption property between NO_2 and graphene also made recover time longer rather than that of NH_3 as shown in Fig. 3a-b. Consequently, selectivity of NO_2 to NH_3 was effectively enhanced by the decoration of Al NPs while Pd NPs slightly improved NH_3 selectivity to NO_2 (see Fig. S4a in the SI). However, the sensor with thicker metal film exhibited lower or negligible gas responses due to a major conduction path through the metal film rather than graphene channel (data not shown here).[37] On the one hand, if perfect monolayer or nano-ribbon graphene can be implemented, much higher sensitivity would be obtained in gas sensing devices.[12,38] Preliminarily, we roughly investigated graphene edge effect in gas sensitivity as shown in Fig. S4 in the SI. We observed that overall sensitivities of NO_2 or NH_3 were increased in the patterned graphene devices and gas selectivity in metal-decorated graphene devices was also further enhanced. It means that line-edges of patterned graphene function as additional molecule adsorption sites, contributing to increase of gas reaction sites. Nano-scaled graphene ribbon would be another approach to extremely improve the gas sensing performance.

To scrutinize roles of metal decoration in electronic properties of graphene, we performed 4-probe Hall measurement by Van der Pauw method at room temperature for graphene-based films and compared critical parameters of each film as shown in Fig. 4a. Key parameters, we are mainly concerned with, are mobility and carrier concentration among several parameters extracted from the Hall measurement (for more details, see Table S1 of SI). All the films were observed to show p-type behavior in which major carrier is hole. Such a high carrier density of ~10^{19} might also originate from the effects of multilayer graphene. When compared to the graphene film, Pd NPs decreased hole mobility on graphene. Al NPs, however, increased its hole mobility (left Y-axis of Fig. 4a). Interestingly, carrier concentration showed opposite tendency, i.e., increase for Pd:Graphene and decrease for Al:Grpahene (right Y-axis in Fig. 4a). Overall, as carrier concentration increases, hole mobility decreases, indicating carrier scattering is dominant factor to determine the mobility. It should be specially noted that the change in the electrical parameters was found to be more obvious in the Al:Graphene film than the Pd:Graphene. Significant decrease in total hole concentration of Al:Graphene may be caused by the formation of hole depletion region at the interface due to electron transfer from Al NPs to graphene (i.e., n-doping effect). On the other hand, electron transfer would occur from graphene to Pd NPs (i.e., p-doping effect).

It is also important for understanding sensing characteristics to investigate the change of electrical contact properties between graphene channel and metal electrodes. Thus, we have measured current-voltage (I-V) electrical characteristics of each different device as shown in Fig. 4b. Graphene device exhibits non-linear at a voltage sweep in the range of ±1 V, implying the existence of Schottky barrier formed between the Au/Ti metal contact and the graphene channel. In the case of Al:Graphene, the Schottky contact was also retained; however, current level became relatively smaller than Graphene device. As shown in Fig. 4b, Pd:Graphene device showed ohmic I-V behavior. From those I-V characteristics, it can be readily expected that n-doping of Al further raises the Schottky barrier height, which in turn reduce the current flow between graphene and electrodes. Contrarily, p-doping of Pd on graphene film lowers the Schottky barrier height, leading to an ohmic contact. Consequently, the metal decoration on the graphene modulated not only electronic properties (specifically, carrier concentration and mobility) of the graphene itself (Fig. 4a) but also contact properties between metal electrode and channel (Fig. 4b). The change in electrical properties of graphene devices after metal decoration may influence sensing characteristics.

It has been generally accepted that metal decoration on sensing materials can improve the sensitivity to specific analyte gas molecules, which has been explained by chemical sensitization or electronic sensitization.[39] Particularly, in the chemical sensitization effect, decoration of metal NPs on sensing film increases the overall active sensing surface area and the subsequent adsorption sites of gas molecules. However, in our case, Al NPs increased the sensitivity to NO_2 but Pd NPs decreased the sensitivity to NO_2. For NH_3 gas, it shows different behavior in sensing characteristic. Therefore, it is not reasonable to conclude that change in the sensor sensitivity can be only attributed to the increased adsorption sites of gas molecule. Alternatively, electronic sensitization can be considered as possible underlying mechanism of the sensitivity tuning for each different metal.[39] As listed in Table S1 in SI, graphene is normally p-dominant conducting properties due to adsorbed water and oxygen molecules under ambient condition.[34] As shown in the experimental observation, resistivity increase (specifically, decrease in carrier concentration) of the graphene after Al NPs decoration suggests the formation of a hole depletion region of the graphene film near the interface with Al NPs, which is corresponded with the Schottky junction formed owing to large Fermi level difference between metal Al and p-type semiconducting graphene.[40] The hole depletion at the interface facilitates the electron charge transfer from graphene to NO_2 molecules, improving the sensing characteristics to NO_2; however, fewer electrons are transferred from NH_3 molecules to graphene, showing the suppressed response to NH_3. Meanwhile, it was experimentally observed that graphene after Pd NPs decoration shows increased hole concentration. Note that Pd is a high work function metal and thus the adsorption of Pd NPs on the graphene is expected to induce the formation of hole carriers.[40] Hole accumulation at the interface due to p-doping effect of Pd on graphene limits electron charge transfer from graphene to NO_2 molecules, decreasing response to NO_2; however, gas response to NH_3 would be somewhat improved. Consequently, graphene hybrid structures modify the electronic properties of graphene-based sensors, which in turn modulates gas sensing characteristics. Electronic sensitization effect of the doped graphenes could result in the selective response to specific analyte gas. Nevertheless, deep understanding of the gas sensing mechanism in graphene-metal hybrid system is considerably intricate and needs further studies.

In order to investigate the potential capability to flexible gas sensor, we also fabricated two different devices (Graphene and Al:Graphene on PI substrate) and compared sensing properties of each device under 1.2 ppm NO_2 gas flow. Operating temperature was set to ~150 °C which is the same condition for testing gas sensing characteristics of the devices fabricated on hard substrate. Because glass transition temperature of the PI film used is higher enough than the operating temperature, its mechanical and chemical degradation would be avoided during gas sensing test. In initial test before bending, the Al:Graphene device on PI substrate showed 270 % increased sensitivity compared to the Graphene device (Fig. 5a), which is well

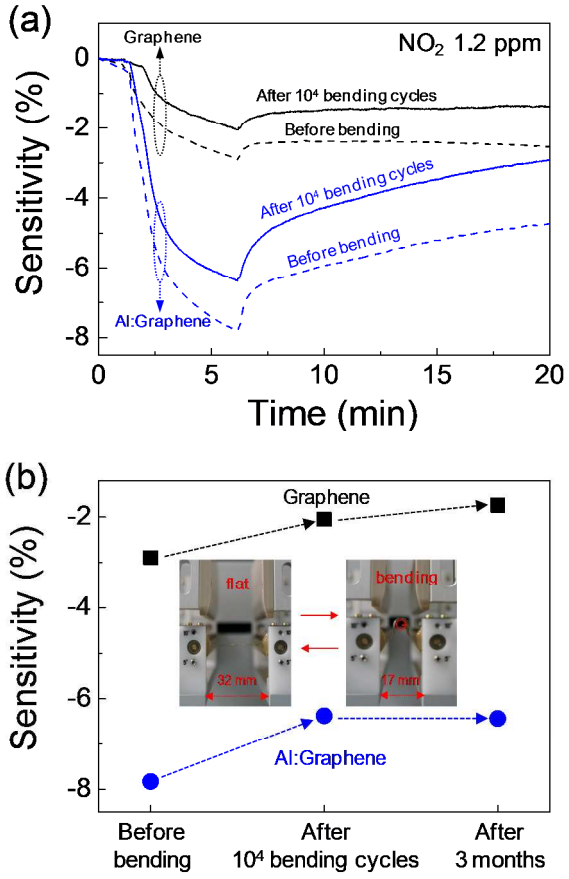

Fig. 5 (a) Transient response characteristics for both Graphene and Al:Graphene flexible gas sensing devices under 1.2 ppm of NO_2 gas before/after 10^4 bending cycles. (b) Comparison of sensitivity change for both Graphene and Al:Graphene flexible gas sensing devices after bending test and then 3 months; inset: optical image showing the bending test condition. All the gas sensing test was performed at the operating temperature of 150 °C.

consistent with the result found in the devices on SiO_2/Si substrate. Resistance change as function of bending radius was negligible (see Fig. S5a in the SI) but in the bending cycling test, some fluctuation in resistance value was observed after 5000 cycles (see Fig. S5b in the SI). Continuous stress during the bending test would lead to irrecoverable deformation on the grain boundaries between graphene domains. Most cracks also start to evolve in the grain boundary regions.[41] The stress-induced permanent deformation on the grain boundaries and macroscopic cracks might increase the resistance of the flexible graphene device. Even though NO_2 gas response for both devices became slightly degraded after 10^4 bending cycles, compared to the Graphene device, considerable sensitivity enhancement of Al:Graphene device was achieved as shown in Fig. 5a. The sensitivity values of each device before and after bending were extracted as displayed in Fig. 5b. Both devices somewhat experienced slight degradation of sensitivity which might be caused by the mechanical deformation of graphene film itself after bending test. Long-term stability after 3 months was also reasonably maintained as shown in Fig. 5b. The highly sensitive and reliable flexible graphene-based gas sensor will pave a simple way toward practical gas sensor applications.

Conclusions

We have investigated the effect of metal decorations on the sensing characteristics of graphene-based devices for NO_2 and NH_3, and demonstrated flexible gas sensor application as well. Experimental results clearly validate that Pd NPs on the graphene accumulate hole carriers of graphene, resulting in the gas sensor sensitized by NH_3 gas molecular adsorption On the contrary, Al NPs deplete hole carriers, which improves dramatically NO_2 sensitivity. The synergistic combination between metal NPs and graphene modulates the electronic properties of graphene, which in turn significantly enhances selectivity and sensitivity in gas sensing characteristics. Sensitivity of flexible graphene-based gas sensor was enhanced by same approach even after 10^4 bending cycles. Furthermore, long-term stability after 3 months was also obtained. It would be a promising and simple route for tuning the gas sensor selectivity in practical applications.

Acknowledgements

This work was supported by the research fund of the Korea Institute of Materials Science and also by the "Gyeongsangnam, Changwon Science Research Park Project" of the Grant of the Korean Ministry of Science, ICT and Future Planning.

Notes and references

[a]Advanced Functional Thin Films Department, Surface Technology Division, Korea Institute of Materials Science (KIMS), Changwon, Gyeongnam 641-831, Republic of Korea, *E-mail: bjcho@kims.re.kr
[b]School of Materials Science and Engineering, Gwangju Institute of Science and Technology (GIST), Gwangju 500-712, Republic of Korea
[c]Department of Physics Education, Chonnam National University, Gwangju 500-757, Republic of Korea

† Electronic Supplementary Information (ESI) available: See DOI: 10.1039/b000000x/

1. A. K. Geim and K. S. Novoselov, *Nat. Mater.*, 2007, **6**, 183–191.
2. C. Lee, X. Wei, J. W. Kysar, and J. Hone, *Science*, 2008, **321**, 385–388.
3. D. C. Elias, R. R. Nair, T. M. G. Mohiuddin, S. V Morozov, P. Blake, M. P. Halsall, a C. Ferrari, D. W. Boukhvalov, M. I. Katsnelson, a K. Geim, and K. S. Novoselov, *Science*, 2009, **323**, 610–613.
4. A. A. Balandin, *Nat. Mater.*, 2011, **10**, 569–581.
5. H. Yan, T. Low, W. Zhu, Y. Wu, M. Freitag, X. Li, P. Avouris, and F. Xia, *Nat. Photonics*, 2013, **7**, 394–399.
6. F. Schwierz, *Nat. Nanotechnol.*, 2010, **5**, 487–496.
7. Y. Wu, Y. Lin, A. A. Bol, K. A. Jenkins, F. Xia, D. B. Farmer, Y. Zhu, and P. Avouris, *Nature*, 2011, **472**, 74–78.
8. J. Wu, W. Pisula, and K. Müllen, *Chem. Rev.*, 2007, **107**, 718–747.
9. Y. Sun, Q. Wu, and G. Shi, *Energy Environ. Sci.*, 2011, **4**, 1113–1132.
10. X. Gan, R.-J. Shiue, Y. Gao, I. Meric, T. F. Heinz, K. Shepard, J. Hone, S. Assefa, and D. Englund, *Nat. Photonics*, 2013, **7**, 883–887.
11. Z.-S. Wu, S. Pei, W. Ren, D. Tang, L. Gao, B. Liu, F. Li, C. Liu, and H.-M. Cheng, *Adv. Mater.*, 2009, **21**, 1756–1760.
12. F. Schedin, A. K. Geim, S. V Morozov, E. W. Hill, P. Blake, M. I. Katsnelson, and K. S. Novoselov, *Nat. Mater.*, 2007, **6**, 652–655.
13. H. Vedala, D. C. Sorescu, G. P. Kotchey, and A. Star, *Nano Lett.*, 2011, **11**, 2342–2347.
14. J. K. Wassei and R. B. Kaner, *Mater. Today*, 2010, **13**, 52–59.
15. S. Srivastava, K. Jain, V. N. Singh, S. Singh, N. Vijayan, N. Dilawar, G. Gupta, and T. D. Senguttuvan, *Nanotechnology*, 2012, **23**, 205501.
16. A. Gutés, B. Hsia, A. Sussman, W. Mickelson, A. Zettl, C. Carraro, and R. Maboudian, *Nanoscale*, 2012, **4**, 438–440.
17. R. K. Paul, S. Badhulika, N. M. Saucedo, and A. Mulchandani, *Analytical chemistry*, 2012, **84**, 8171–8178.
18. F. Yavari and N. Koratkar, *J. Phys. Chem. Lett.*, 2012, **3**, 1746–1753.
19. F. Yavari, Z. Chen, A. V Thomas, W. Ren, H.-M. Cheng, and N. Koratkar, *Sci. Rep.*, 2011, **1**, 166.
20. V. Tjoa, W. Jun, V. Dravid, S. Mhaisalkar, and N. Mathews, *J. Mater. Chem. C*, 2011, **21**, 15593–15599.
21. Y.-H. Zhang, Y.-B. Chen, K.-G. Zhou, C.-H. Liu, J. Zeng, H.-L. Zhang, and Y. Peng, *Nanotechnology*, 2009, **20**, 185504.
22. X. Zhou, X. Wang, B. Wang, Z. Chen, C. He, and Y. Wu, *Sensors and Actuators B*, 2014, **193**, 340–348.
23. S. Basu and P. Bhattacharyya, *Sensors and Actuators B*, 2012, **173**, 1–21.
24. W. Li, X. Geng, Y. Guo, J. Rong, Y. Gong, L. Wu, X. Zhang, P. Li, J. Xu, G. Cheng, M. Sun, and L. Liu, *ACS nano*, 2011, **5**, 6955–6961.
25. J. T. Robinson, F. K. Perkins, E. S. Snow, Z. Wei, and P. E. Sheehan, *Nano Lett.*, 2008, **8**, 3137–3140.
26. C. Thomsen and S. Reich, *Phys. Rev. Lett.*, 2000, **85**, 5214–5217.
27. E. Kayhan, R. M. Prasad, A. Gurlo, O. Yilmazoglu, J. Engstler, E. Ionescu, S. Yoon, A. Weidenkaff, and J. J. Schneider, *Chem. Eur. J.*, 2012, **18**, 14996–15003.
28. M. A. Pimenta, G. Dresselhaus, M. S. Dresselhaus, L. G. Cançado, A. Jorio, and R. Saito, *Phys. Chem. Chem. Phys.*, 2007, **9**, 1276–1291.
29. L. Cançado, A. Reina, J. Kong, and M. Dresselhaus, *Phys. Rev. B*, 2008, **77**, 245408.
30. X. Li, W. Cai, J. An, S. Kim, J. Nah, D. Yang, R. Piner, A. Velamakanni, I. Jung, E. Tutuc, S. K. Banerjee, L. Colombo, and R. S. Ruoff, *Science*, 2009, **324**, 1312–1314.
31. Y. Zhang and H. Dai, *Appl. Phys. Lett.*, 2000, **77**, 3015–3017.
32. Y. Zhang, N. W. Franklin, R. J. Chen, and H. Dai, *Chem. Phys. Lett.*, 2000, **331**, 35–41.
33. S. Prezioso, F. Perrozzi, L. Giancaterini, C. Cantalini, E. Treossi, V. Palermo, M. Nardone, S. Santucci, and L. Ottaviano, *J. Phys. Chem. C*, 2013, **117**, 10683–10690.
34. I. Jung, D. a Dikin, R. D. Piner, and R. S. Ruoff, *Nano Lett.*, 2008, **8**, 4283–4287.
35. M. Zhou, Y.-H. Lu, Y.-Q. Cai, C. Zhang, and Y.-P. Feng, *Nanotechnology*, 2011, **22**, 385502.
36. M. Zhou, Y.-H. Lu, Y.-Q. Cai, C. Zhang, and Y.-P. Feng, *Nanotechnology*, 2011, **22**, 385502.
37. M. Gyun, D. Kim, D. Kyun, T. Kim, H. Uk, H. Myoung, J. Yoo, S. Hong, T. June, and Y. Hyup, *Sensors and Actuators B*, 2012, **169**, 387–392.
38. M. Han, B. Özyilmaz, Y. Zhang, and P. Kim, *Phys. Rev. Lett.*, 2007, **98**, 206805.
39. M. E. Franke, T. J. Koplin, and U. Simon, *Small*, 2006, **2**, 36–50.
40. B.-K. Kim, N. Park, P. S. Na, H.-M. So, J.-J. Kim, H. Kim, K.-J. Kong, H. Chang, B.-H. Ryu, Y. Choi, and J.-O. Lee, *Nanotechnology*, 2006, **17**, 496–500.
41. J. Zhang, J. Zhao, and J. Lu, *ACS nano*, 2012, **6**, 2704–2711.

Graphical abstract

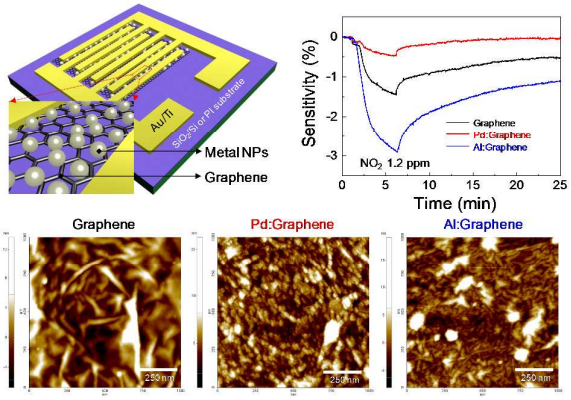

Synergistic combination of metal nanoparticles and graphene modulates electronic properties of graphene, leading to enhancement in gas sensitivity and selectivity.